UF College of Public Health and Health Professions
Department of Environmental and Global Health
UNIVERSITY *of* FLORIDA

Integrating Machine Learning and Quantitative Structure-Activity Relationships (QSAR) Modeling Approaches to Develop Artificial Intelligence (AI)-assisted Interactive Physiologically Based Pharmacokinetic (iPBPK) Modeling Web Dashboard.

---- RASS/BMSS/AACT Joint Webinar
---- December 13th, 2023

Wei-Chun Chou

Center for Environmental and Human Toxicology (CEHT)
Department of Environmental and Global Health, College of Public Health and Health Professions
University of Florida, Gainesville, FL 32610

Case studies

A. Development of Artificial Intelligence (AI)-Assisted PBPK Model in Cancer Nanomedicine

B. Development of a Multi-Organ Toxicity Predictive Model Using Multi-Task Learning in Deep Neural Network

Case studies

A. **Development of Artificial Intelligence (AI)-Assisted PBPK Model in Cancer Nanomedicine**

B. **Development of a Multi-Organ Toxicity Predictive Model Using Multi-Task Learning in Deep Neural Network**

Challenge in tumor delivery of nanomedicine

- The poor tumor delivery efficiency of nanomedicines has been a major barrier in the translation of nanomedicine to potent drug candidates.

- NPs are becoming an increasingly popular tool for biomedical imaging and drug delivery.

- Lack of understanding of pharmacokinetic of nanomedicine might be a major reason.

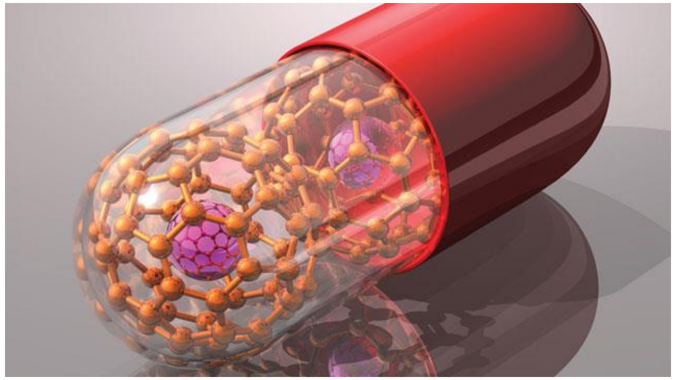

Image source: https://www.the-scientist.com/cover-story/nanomedicine-37087

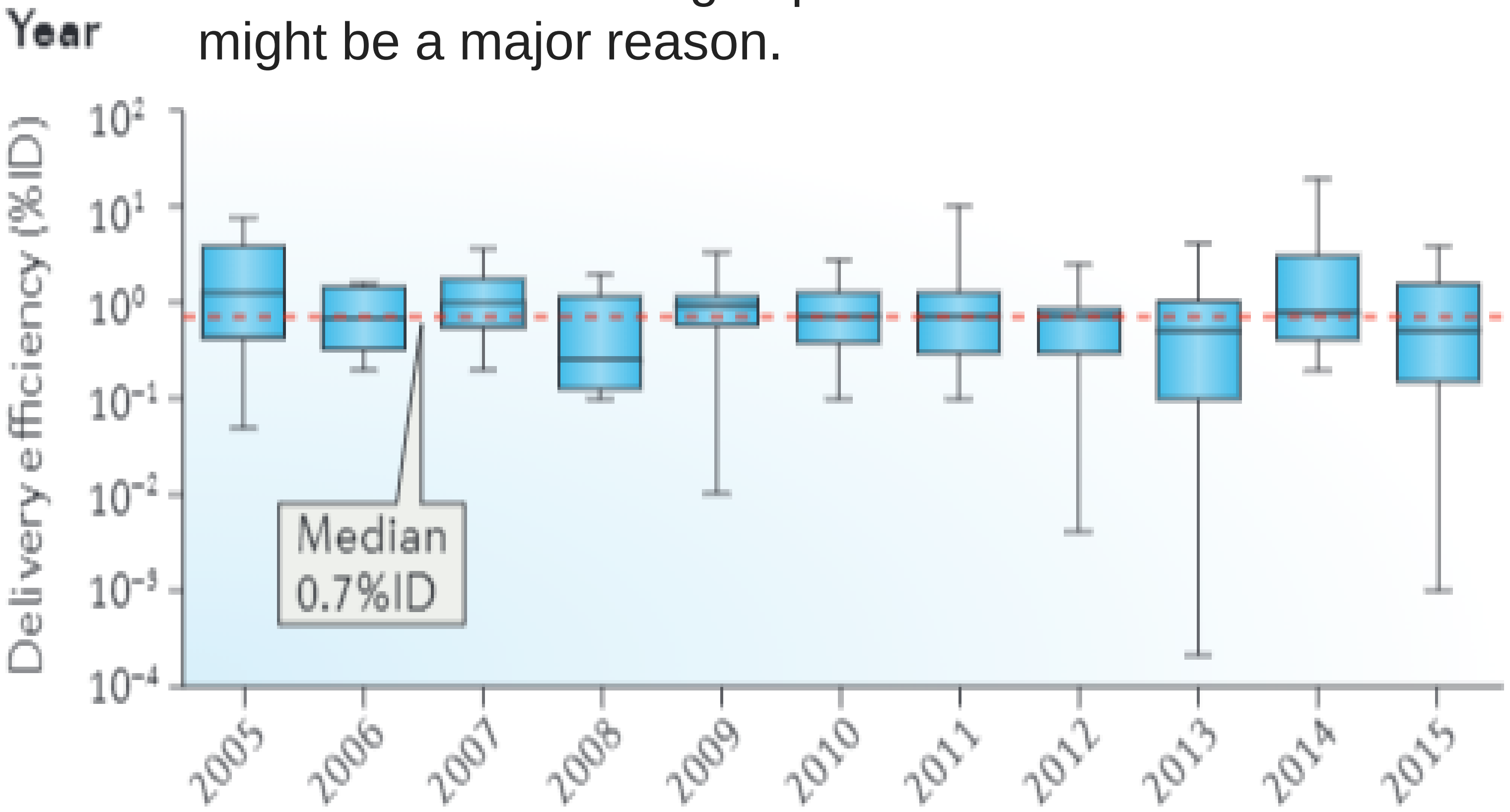

Image was obtained from Wilhelm et al., 2016

Abbreviations: Nanoparticles (NPs)

Biodistribution of Nanoparticles (NPs)

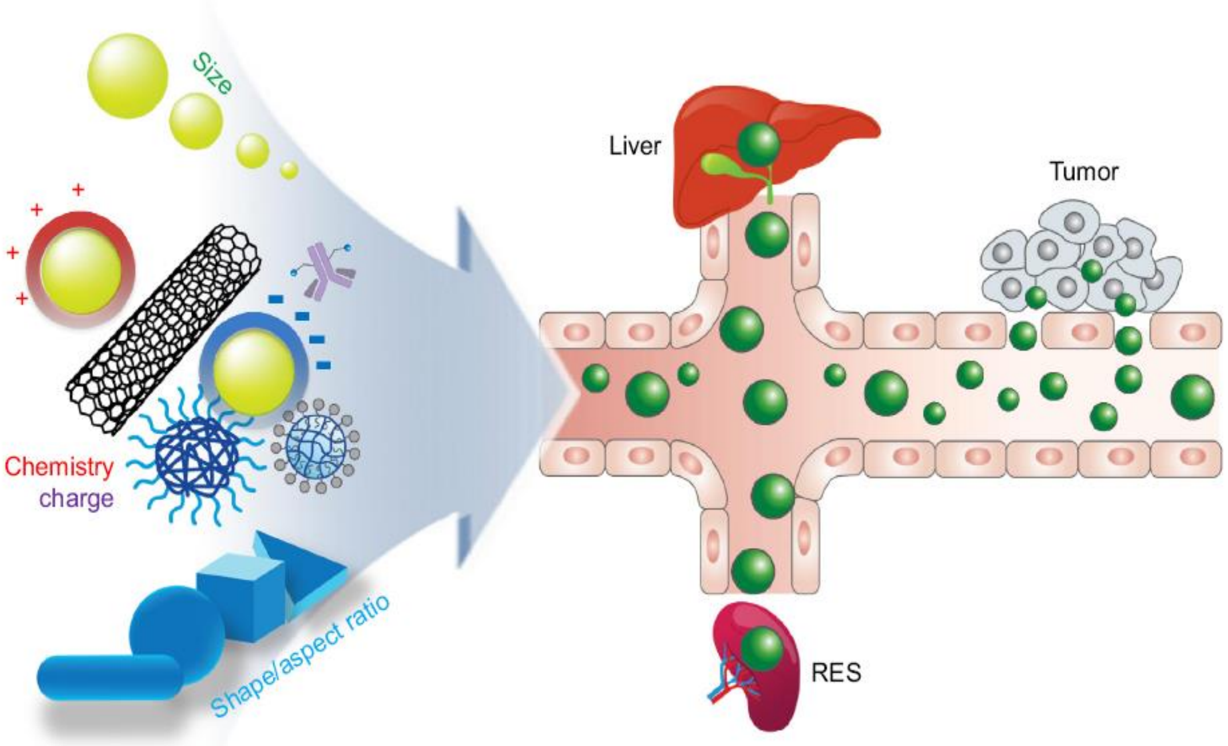

Reticuloendothelial System (RES)

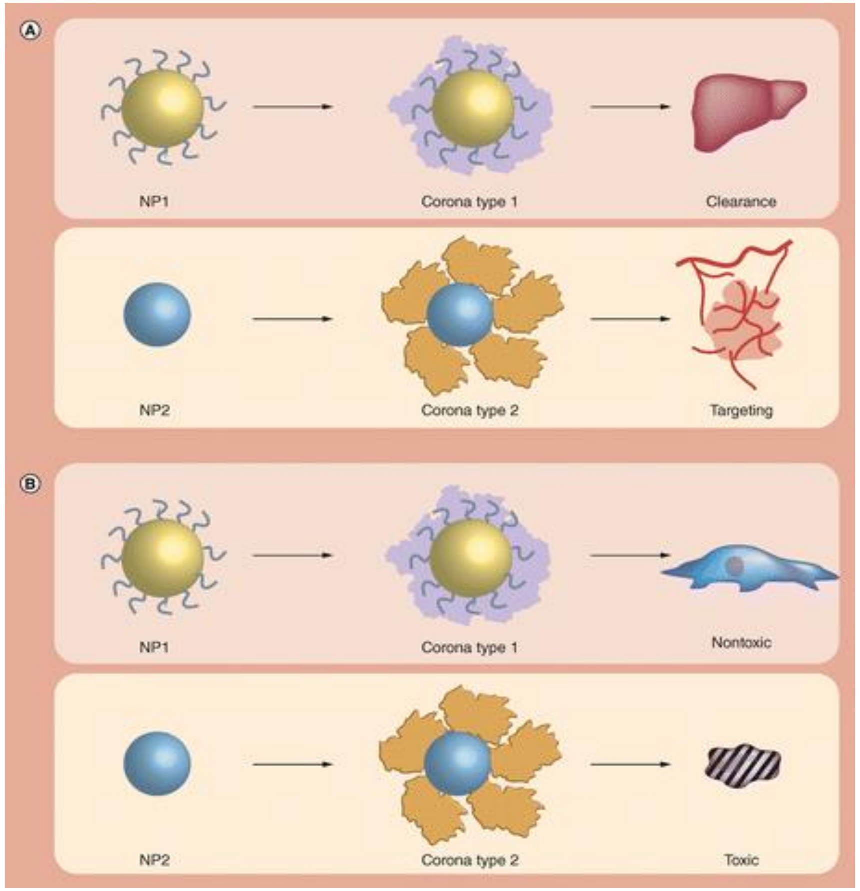

- The pharmacokinetics of nanomedicine is very different with the traditional drugs.
- One of important mechanisms to affect the NPs' biodistribution is **phagocytosis.**
- Different physicochemical properties of NPs, such as size, materials, biochemistry, and shape, may relate to the NPs' phagocytosis and biodistribution.

Kim et al., 2015; Hamad-Schifferli et al., 2015

Theoretical parameter: Endocytosis of NPs

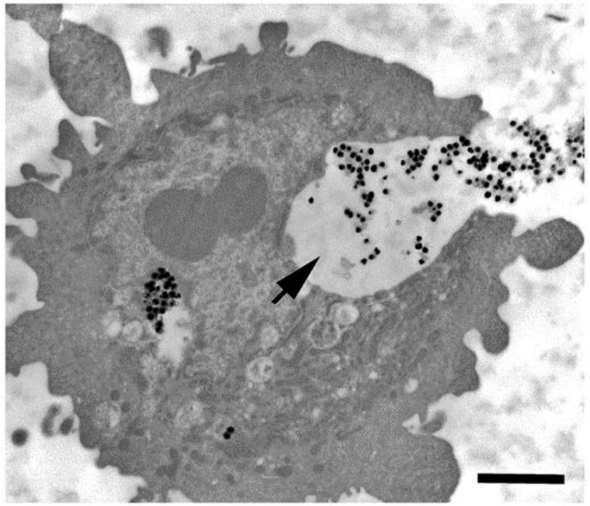

Monteiro-Riviere et al. 2013. Toxicology Letters

- Hill function to simulate endocytosis of gold nanoparticles

$$K_{up,i}(t) = \frac{K_{max,i} \times t^{n_i}}{t_{50,i}^{n_i} + t^{n_i}}$$

$K_{max,i}$: maximum uptake rate

$K_{50,i}$: time reaching half maximum rate

n_i: Hill coefficient

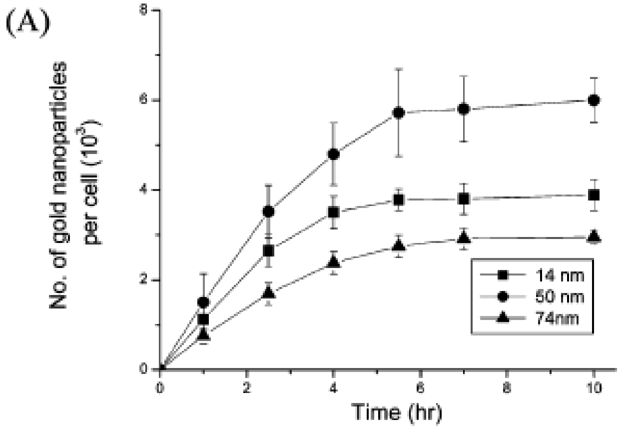

Chithrani et al. 2006. Nano Letters

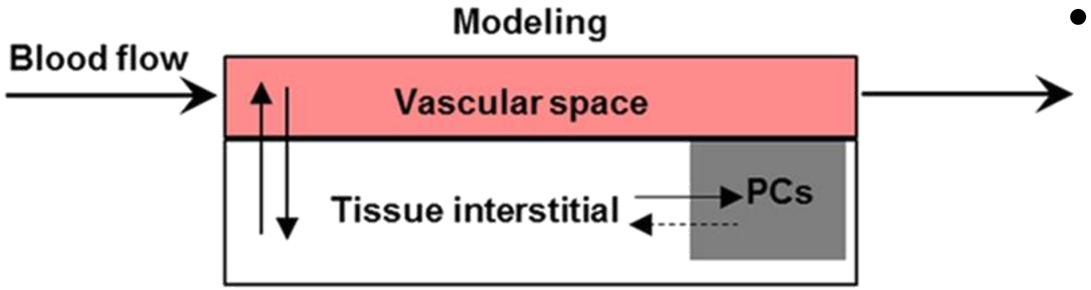

- Simplified equation in PBPK model

$$\frac{dA_{T_i}}{dt} = -K_{up_i} \times A_{T_i} + K_{re,i} \times A_{PC_i}$$

Lin et al., 2016. Nanotoxicology

PCs represent phagocytic cells in organs or tumors;
A_(Ti) represents amount of NPs in the tissue interstitium of the organ;
Kre,i is the release rate constant of NMs by PCs
Physiological based pharmacokinetic (PBPK) model

A hybrid method (AI-assisted PBPK model)

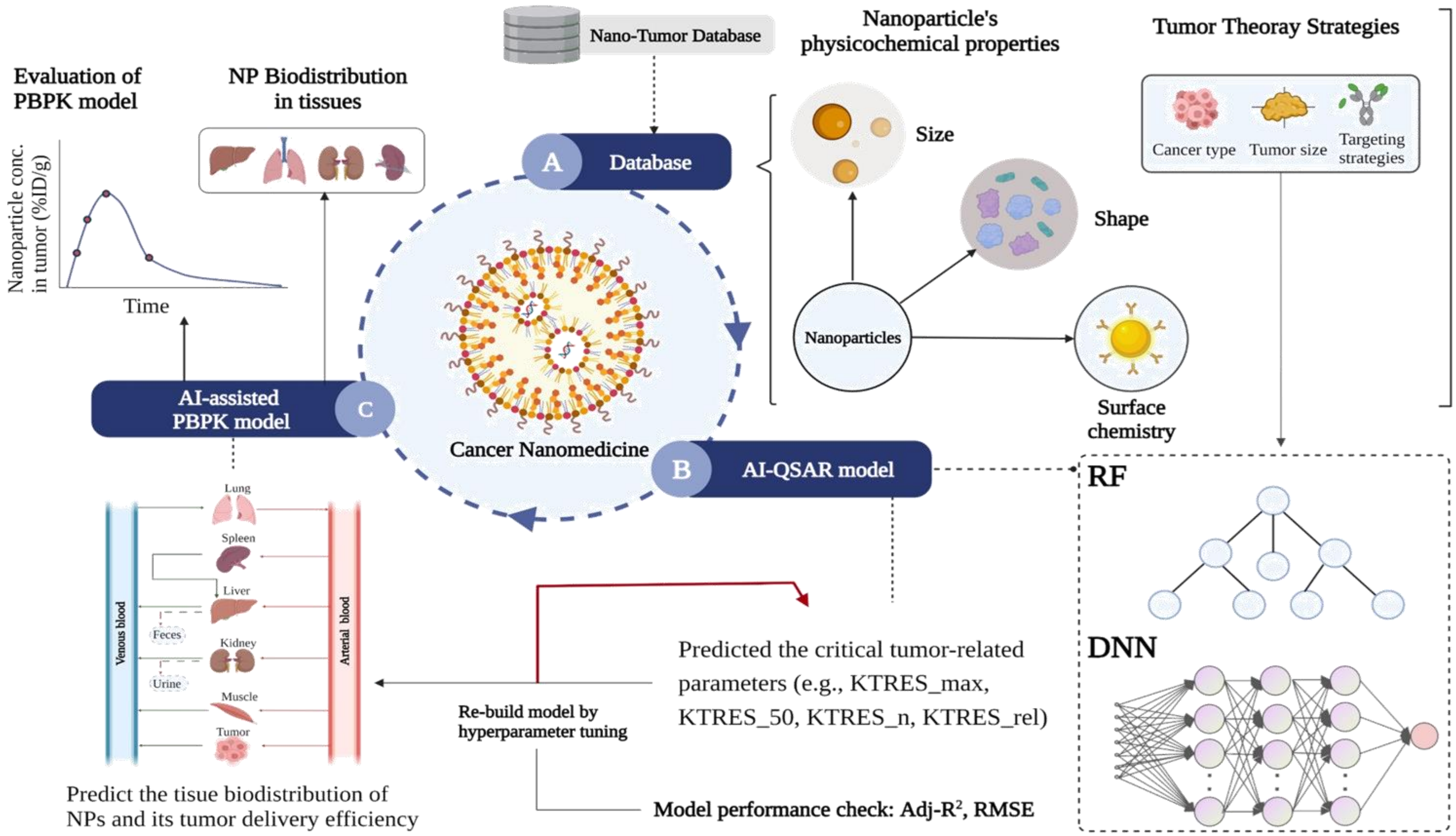

Chou WC, Chen Q, Yuan L, Cheng YH, He C, Monteiro-Riviere NA, Riviere JE, Lin Z. An artificial intelligence-assisted physiologically-based pharmacokinetic model to predict nanoparticle delivery to tumors in mice. J Control Release. 2023 Sep;361:53-63

Variables in the Nano-Tumor Database

1. Categorical variables

- Material: Inorganic/organic NPs →1/0
- Shape: Spherical/Rod/circle → 1…3
- Cancer type: Brain/Breast/…
- Tumor model (TM)
- Targeting strategy (TS): Active/Passive →1/0

2. Numerical variables

- Hydrodynamic diameter [nm]
- Zeta potential [mV]

3. Target variables

- Critical Kinetic parameters related to phagocytosis

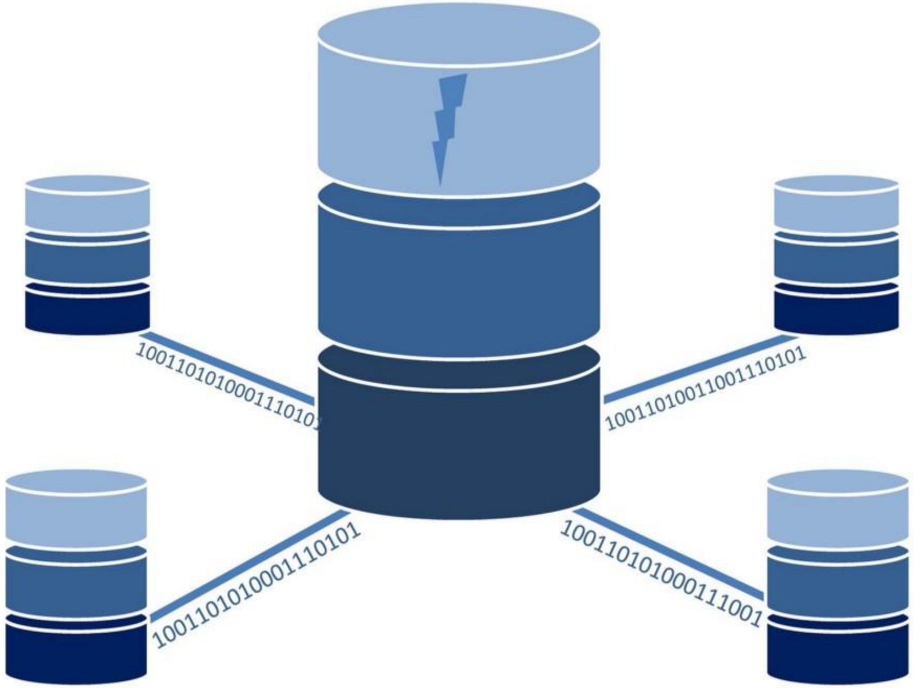

Image by Tumisu from Pixabay

Development of AI-QSAR model

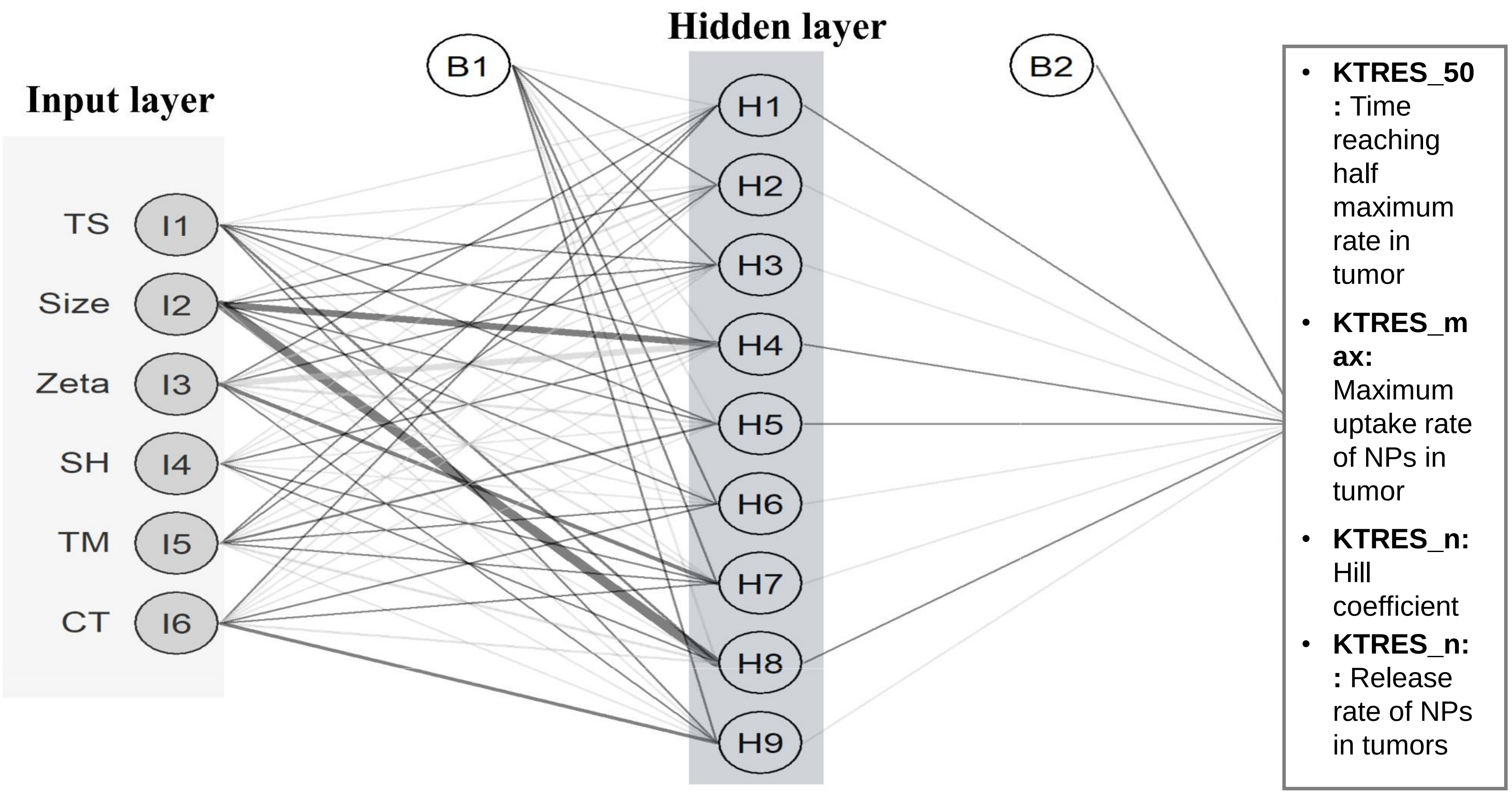

1. To avoid overfitting, we constrained the model architecture to 3 layers, which of the layers contain lower than 512 nodes
2. Shuffled 5-fold cross-validation was used to test the generalization of the model.
3. Bayesian optimization was used to tune the hyper-parameters of the models.

PBPK model for tumor-bearing mice

Physiological based pharmacokinetic (PBPK) model for tumor-bearing mice

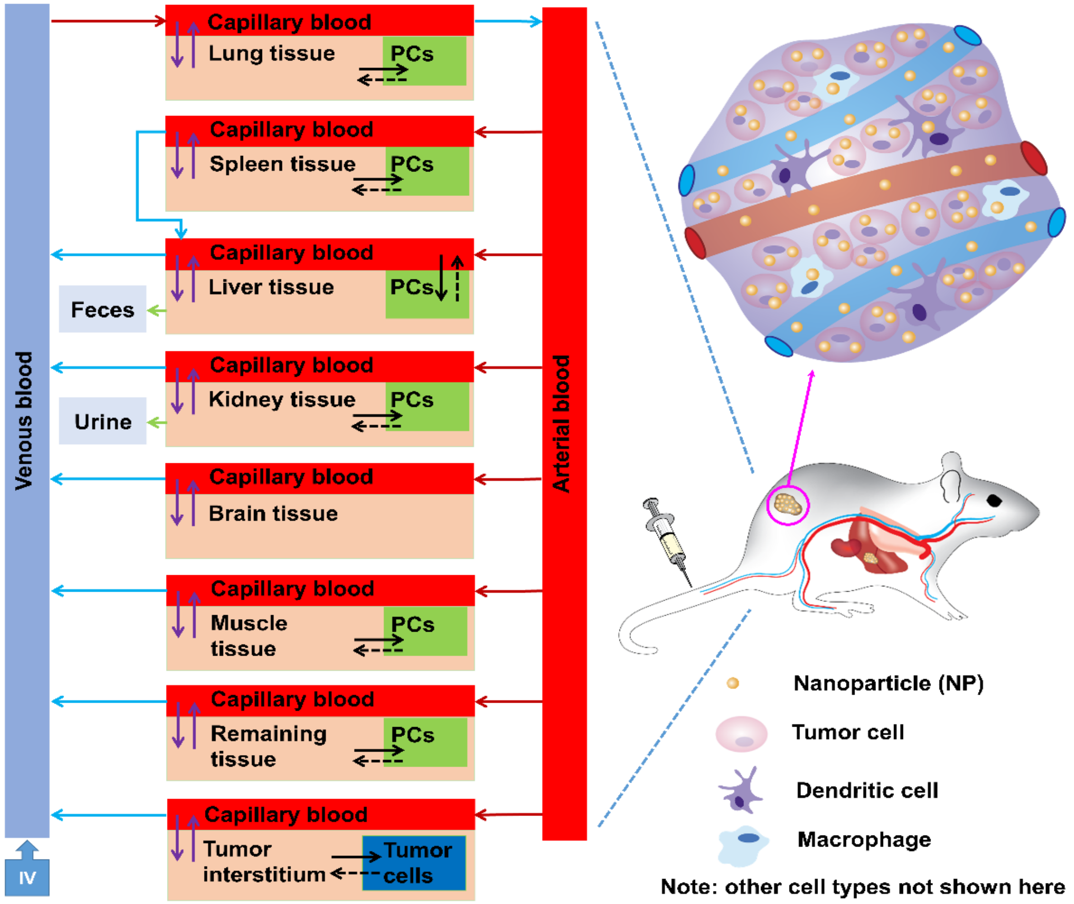

PCs represent phagocytic cells in organs or tumors;

Model fitting with animal studies

Nano Tumor Database: (376 datasets from 200 studies)

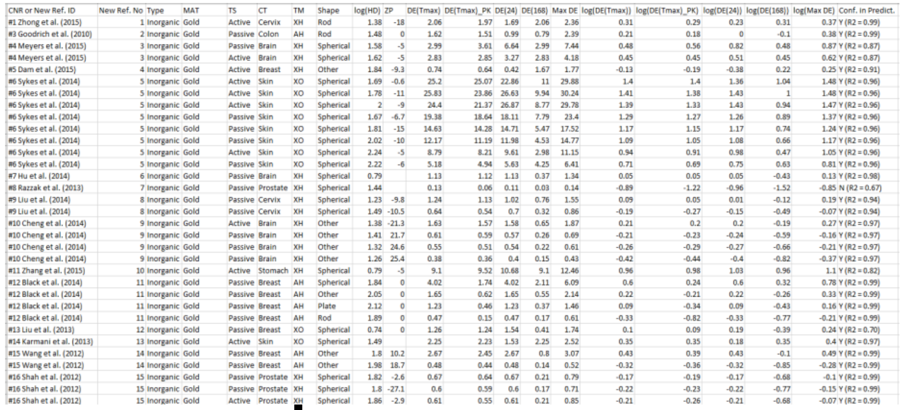

CNR or New Ref. ID	New Ref. No	Type	MAT	TS	CT	TM	Shape	log(HD)	ZP	DE(Tmax)	DE(Tmax)_PK	DE(24)	DE(168)	Max DE	log(DE(Tmax))	log(DE(Tmax)_PK)	log(DE(24))	log(DE(168))	log(Max DE)	Conf. in Predict.
#1 Zhong et al. (2015)	1	Inorganic	Gold	Active	Cervix	XH	Rod	1.38	-18	2.06	1.97	1.69	2.06	2.36	0.31	0.29	0.23	0.31	0.37	Y (R2 = 0.99)
#3 Goodrich et al. (2010)	2	Inorganic	Gold	Passive	Colon	AH	Rod	1.48	0	1.62	1.51	0.99	0.79	2.39	0.21	0.18	0	-0.1	0.38	Y (R2 = 0.99)
#4 Meyers et al. (2015)	3	Inorganic	Gold	Passive	Brain	XH	Spherical	1.58	-5	2.99	3.61	6.64	2.99	7.44	0.48	0.56	0.82	0.48	0.87	Y (R2 = 0.87)
#4 Meyers et al. (2015)	3	Inorganic	Gold	Active	Brain	XH	Spherical	1.62	-5	2.83	2.85	3.27	2.83	4.18	0.45	0.45	0.51	0.45	0.62	Y (R2 = 0.87)
#5 Dam et al. (2015)	4	Inorganic	Gold	Active	Breast	XH	Other	1.84	-9.3	0.74	0.64	0.42	1.67	1.77	-0.13	-0.19	-0.38	0.22	0.25	Y (R2 = 0.91)
#6 Sykes et al. (2014)	5	Inorganic	Gold	Active	Skin	XO	Spherical	1.69	-0.6	25.2	25.07	22.86	11	29.88	1.4	1.4	1.36	1.04	1.48	Y (R2 = 0.96)
#6 Sykes et al. (2014)	5	Inorganic	Gold	Active	Skin	XO	Spherical	1.78	-11	25.83	23.86	26.63	9.94	30.24	1.41	1.38	1.43	1	1.48	Y (R2 = 0.96)
#6 Sykes et al. (2014)	5	Inorganic	Gold	Active	Skin	XO	Spherical	2	-9	24.4	21.37	26.87	8.77	29.78	1.39	1.33	1.43	0.94	1.47	Y (R2 = 0.96)
#6 Sykes et al. (2014)	5	Inorganic	Gold	Passive	Skin	XO	Spherical	1.67	-6.7	19.38	18.64	18.11	7.79	23.4	1.29	1.27	1.26	0.89	1.37	Y (R2 = 0.96)
#6 Sykes et al. (2014)	5	Inorganic	Gold	Passive	Skin	XO	Spherical	1.81	-15	14.63	14.28	14.71	5.47	17.52	1.17	1.15	1.17	0.74	1.24	Y (R2 = 0.96)
#6 Sykes et al. (2014)	5	Inorganic	Gold	Passive	Skin	XO	Spherical	2.02	-10	12.17	11.19	11.98	4.53	14.77	1.09	1.05	1.08	0.66	1.17	Y (R2 = 0.96)
#6 Sykes et al. (2014)	5	Inorganic	Gold	Active	Skin	XO	Spherical	2.24	-5	8.79	8.21	9.61	2.98	11.15	0.94	0.91	0.98	0.47	1.05	Y (R2 = 0.96)
#6 Sykes et al. (2014)	5	Inorganic	Gold	Passive	Skin	XO	Spherical	2.22	-6	5.18	4.94	5.63	4.25	6.41	0.71	0.69	0.75	0.63	0.81	Y (R2 = 0.96)
#7 Hu et al. (2014)	6	Inorganic	Gold	Passive	Brain	XH	Spherical	0.79		1.13	1.12	1.13	0.37	1.34	0.05	0.05	0.05	-0.43	0.13	Y (R2 = 0.98)
#8 Razzak et al. (2013)	7	Inorganic	Gold	Passive	Prostate	XH	Spherical	1.44		0.13	0.06	0.11	0.03	0.14	-0.89	-1.22	-0.96	-1.52	-0.85	N (R2 = 0.67)
#9 Liu et al. (2014)	8	Inorganic	Gold	Passive	Cervix	XH	Spherical	1.23	-9.8	1.24	1.13	1.02	0.76	1.55	0.09	0.05	0.01	-0.12	0.19	Y (R2 = 0.94)
#9 Liu et al. (2014)	8	Inorganic	Gold	Passive	Cervix	XH	Spherical	1.49	-10.5	0.64	0.54	0.7	0.32	0.86	-0.19	-0.27	-0.15	-0.49	-0.07	Y (R2 = 0.94)
#10 Cheng et al. (2014)	9	Inorganic	Gold	Active	Brain	XH	Other	1.38	-21.3	1.63	1.57	1.58	0.65	1.87	0.21	0.2	0.2	-0.19	0.27	Y (R2 = 0.97)
#10 Cheng et al. (2014)	9	Inorganic	Gold	Passive	Brain	XH	Other	1.41	21.7	0.61	0.59	0.57	0.26	0.69	-0.21	-0.23	-0.24	-0.59	-0.16	Y (R2 = 0.97)
#10 Cheng et al. (2014)	9	Inorganic	Gold	Passive	Brain	XH	Other	1.32	24.6	0.55	0.51	0.54	0.22	0.61	-0.26	-0.29	-0.27	-0.66	-0.21	Y (R2 = 0.97)
#10 Cheng et al. (2014)	9	Inorganic	Gold	Passive	Brain	XH	Other	1.26	25.4	0.38	0.36	0.4	0.15	0.43	-0.42	-0.44	-0.4	-0.82	-0.37	Y (R2 = 0.97)
#11 Zhang et al. (2015)	10	Inorganic	Gold	Active	Stomach	XH	Spherical	0.79	-5	9.1	9.52	10.68	9.1	12.46	0.96	0.98	1.03	0.96	1.1	Y (R2 = 0.82)
#12 Black et al. (2014)	11	Inorganic	Gold	Passive	Breast	AH	Spherical	1.84	0	4.02	1.74	4.02	2.11	6.09	0.6	0.24	0.6	0.32	0.78	Y (R2 = 0.99)
#12 Black et al. (2014)	11	Inorganic	Gold	Passive	Breast	AH	Other	2.05	0	1.65	0.62	1.65	0.55	2.14	0.22	-0.21	0.22	-0.26	0.33	Y (R2 = 0.99)
#12 Black et al. (2014)	11	Inorganic	Gold	Passive	Breast	AH	Plate	2.12	0	1.23	0.46	1.23	0.37	1.46	0.09	-0.34	0.09	-0.43	0.16	Y (R2 = 0.99)
#12 Black et al. (2014)	11	Inorganic	Gold	Passive	Breast	AH	Rod	1.89	0	0.47	0.15	0.47	0.17	0.61	-0.33	-0.82	-0.33	-0.77	-0.21	Y (R2 = 0.99)
#13 Liu et al. (2013)	12	Inorganic	Gold	Passive	Breast	XO	Spherical	0.74	0	1.26	1.24	1.54	0.41	1.74	0.1	0.09	0.19	-0.39	0.24	Y (R2 = 0.70)
#14 Karmani et al. (2013)	13	Inorganic	Gold	Active	Skin	XO	Spherical	1.49		2.25	2.23	1.53	2.25	2.52	0.35	0.35	0.18	0.35	0.4	Y (R2 = 0.97)
#15 Wang et al. (2012)	14	Inorganic	Gold	Passive	Breast	AH	Other	1.8	10.2	2.67	2.45	2.67	0.8	3.07	0.43	0.39	0.43	-0.1	0.49	Y (R2 = 0.99)
#15 Wang et al. (2012)	14	Inorganic	Gold	Passive	Breast	AH	Other	1.98	18.7	0.48	0.44	0.48	0.14	0.52	-0.32	-0.36	-0.32	-0.85	-0.28	Y (R2 = 0.99)
#16 Shah et al. (2012)	15	Inorganic	Gold	Passive	Prostate	XH	Spherical	1.82	-2.6	0.67	0.64	0.67	0.21	0.79	-0.17	-0.19	-0.17	-0.68	-0.1	Y (R2 = 0.99)
#16 Shah et al. (2012)	15	Inorganic	Gold	Passive	Prostate	XH	Spherical	1.8	-27.1	0.6	0.59	0.6	0.17	0.71	-0.22	-0.23	-0.22	-0.77	-0.15	Y (R2 = 0.99)
#16 Shah et al. (2012)	15	Inorganic	Gold	Active	Prostate	XH	Spherical	1.86	-2.9	0.61	0.55	0.61	0.21	0.85	-0.21	-0.26	-0.21	-0.68	-0.07	Y (R2 = 0.99)

Obtain optimized model parameters

Finalized PBPK model

Chou WC, Chen Q, Yuan L, Cheng YH, He C, Monteiro-Riviere NA, Riviere JE, Lin Z. An artificial intelligence-assisted physiologically-based pharmacokinetic model to predict nanoparticle delivery to tumors in mice. J Control Release. 2023 Sep;361:53-63

Similarity between predicted and data-driven parameters

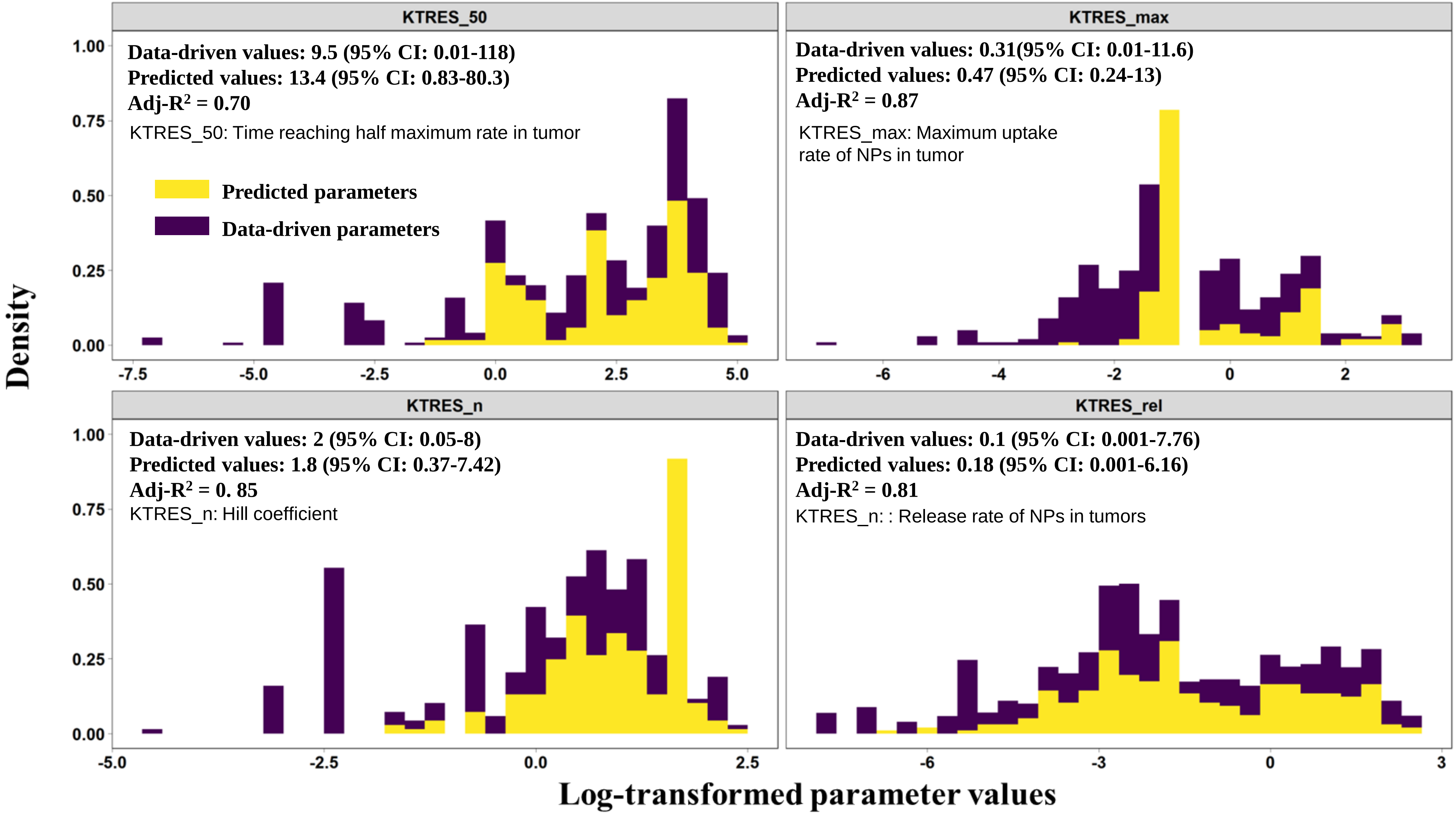

Evaluation results of AI-PBPK model-predicted tumor delivery efficiency

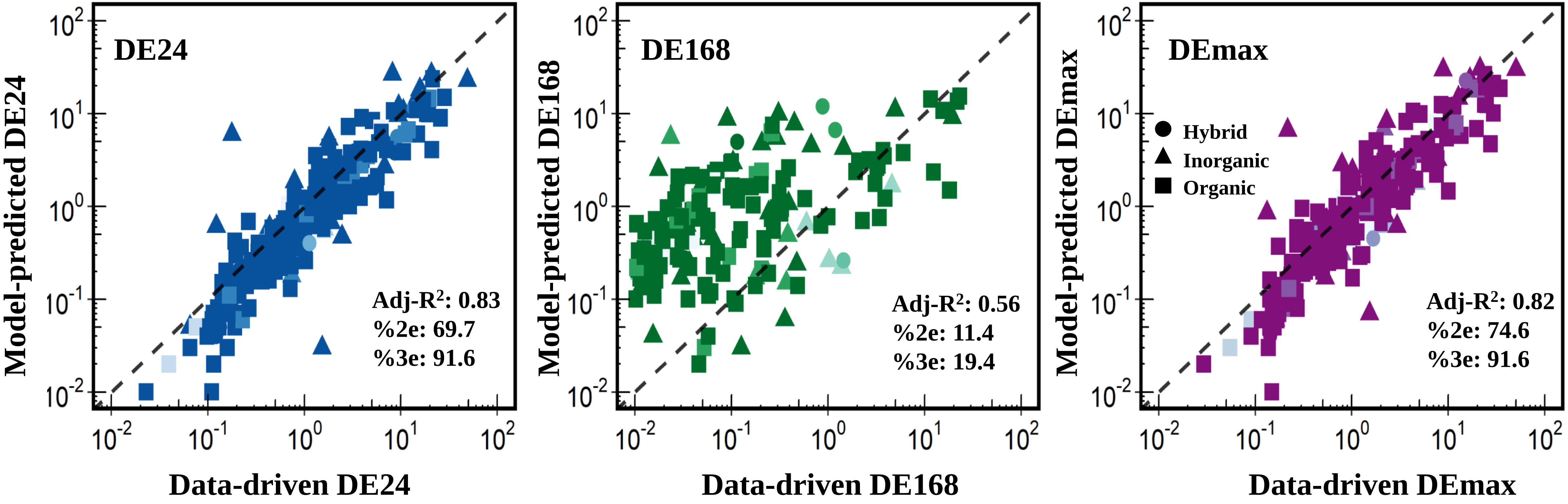

Abbreviation: DE, delivery efficiency; DE24, delivery efficiency at 24 hours;
DE168, delivery efficiency at 168 hours; Demax, maximum of DE;
%2e, percentage of 2-fold error range
%3e, percentage of 3-fold error range

Evaluation results of AI-PBPK model-predicted time-dependent distribution of nanoparticles (NPs) to tumors

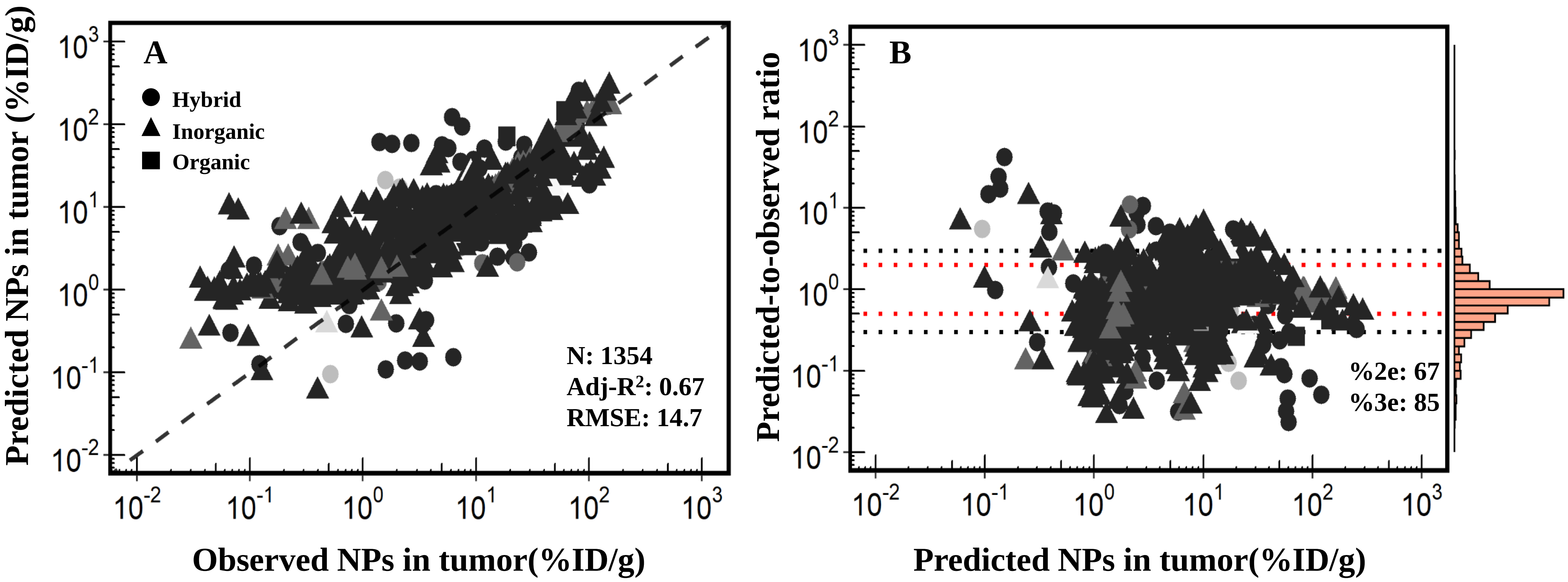

Representative evaluation results of AI-PBPK model

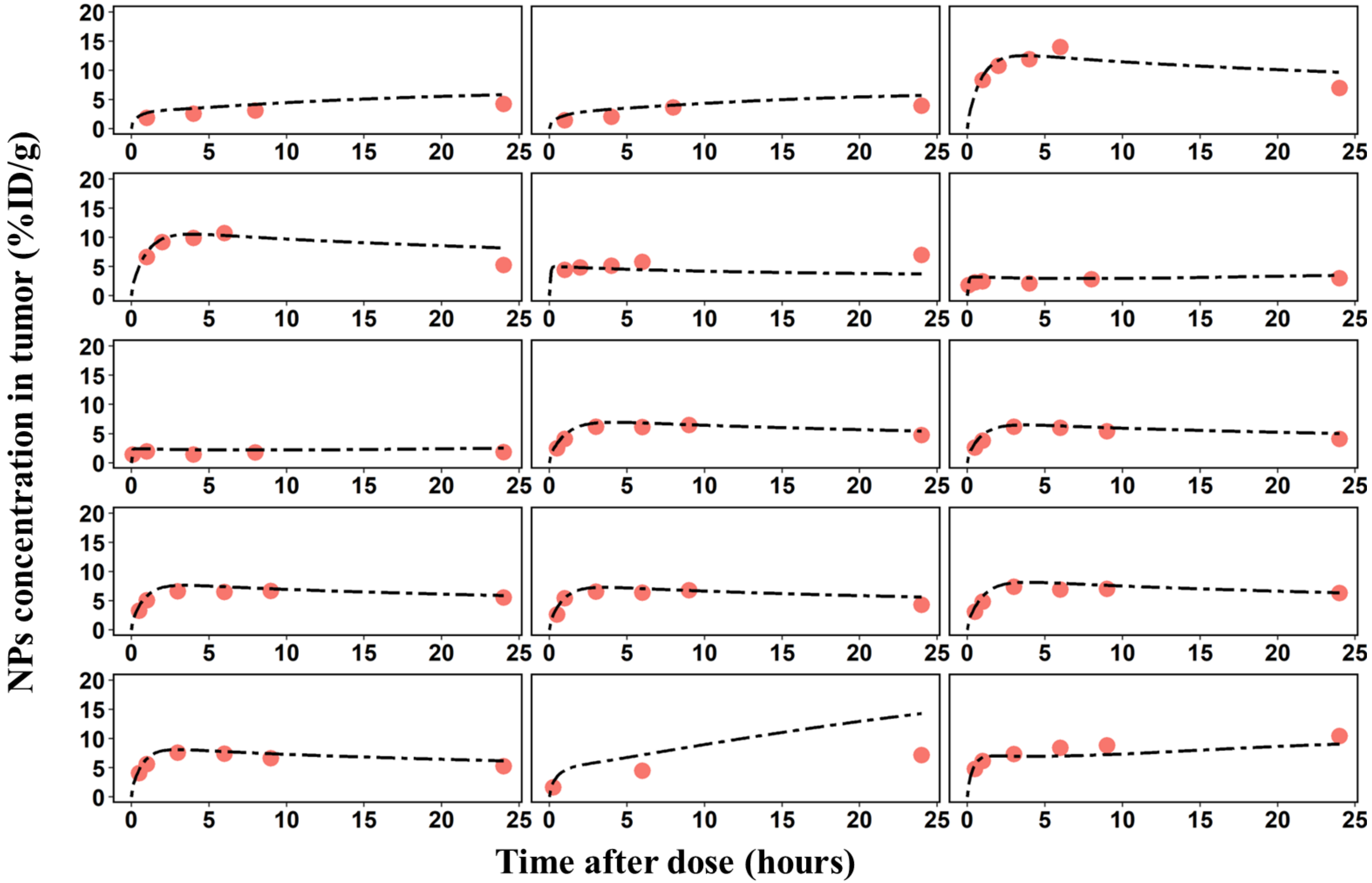

Summary

- This study demonstrated the feasibility of an integration of machine learning/AI technologies with a mechanistic PBPK model to predict the tumor delivery efficiency of NPs.

- Our AI-assisted PBPK model not only provides an early screening tool for estimating tumor delivery efficiency of NPs, but also can reduce the number of animals use at the early-stage preclinical trials to identify NPs with desired delivery efficiency to tumor.

Case studies

A. Development of Artificial Intelligence (AI)-Assisted PBPK Model in Cancer Nanomedicine

B. Development of a Multi-Organ Toxicity Predictive Model Using Multi-Task Learning in Deep Neural Network

Hypothesis

- Drug-induced organ toxicity presents a significant hurdle in drug discovery, potentially impacting multiple organs.
- Existing quantitative structure-activity relationship (QSAR) models predict single toxicity types and overlook systemic toxicity, affecting multiple organs simultaneously.
- Our hypothesis suggests that the multitask-learning QSAR model can overcome the constraints of traditional QSAR models by predicting toxicity across multiple organs.

A schematic of the multi-task QSAR model for the prediction of multi-organ toxicity.

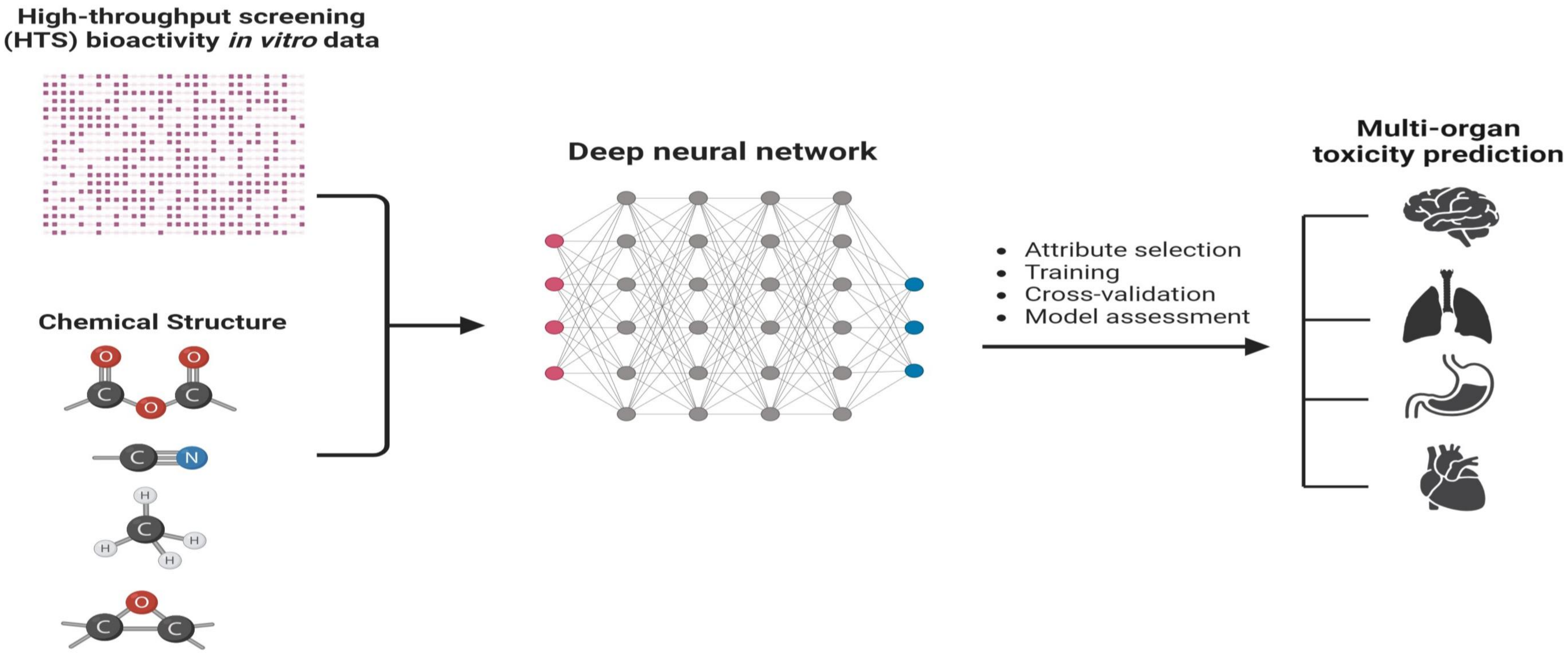

Chou, et al., unpublished results from the Lin Lab at UF.

Materials and Methods

A. In vitro assays and structure data

- The *in vitro* dataset was collected from Tox21 quantitative high-throughput screening (qHTS) data via the National Center for Advancing Translational Sciences (NCTS) website: https://tripod.nih.gov/tox21/assays/
- In this study, we used 72 assays by filtering out the "*Chinese hamster ovary cell lines*" and other "*non-human*" originated cell lines.
- The 1024-bit ECFP4 fingerprints were generated using the Python package "RDKit".

B. Human organ level toxicity data

- Human *in vivo* toxicity data in this study were collected from the studies Xu et al. (2021) and Hu et al., 2022. A total of **2,389** chemicals were collected from the database.
- Six endpoints were chosen which represent different organ-level adverse outcomes, including ***cardiotoxicity***, ***developmental toxicity***, ***hepatotoxicity***, ***nephrotoxicity***, ***neurotoxicity***, and ***reproductive toxicity***.

Density plot of the multi-task QSAR model

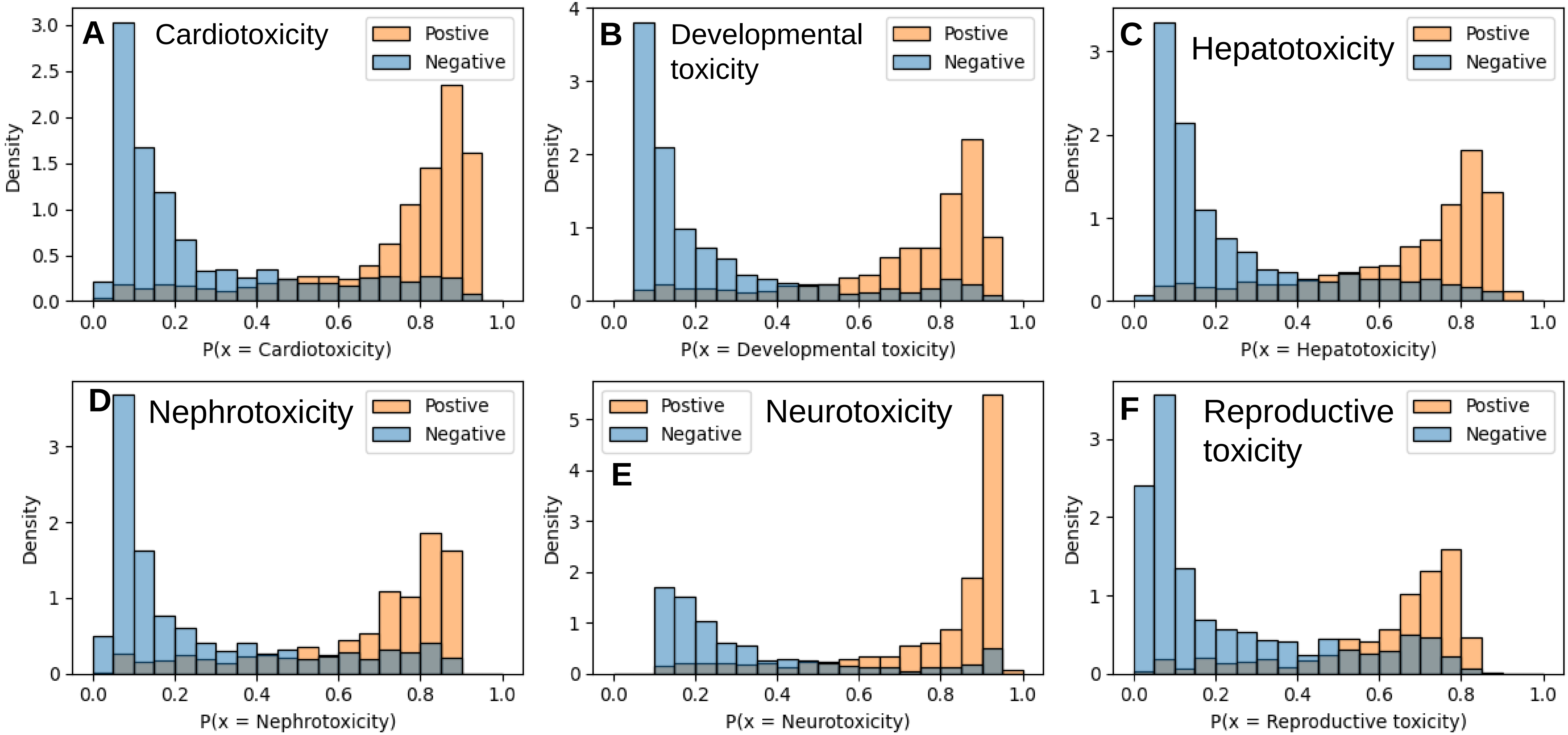

Chou, et al., unpublished results from the Lin Lab at UF.

Receiver operating characteristic curve (ROC) plot of the multi-task QSAR model

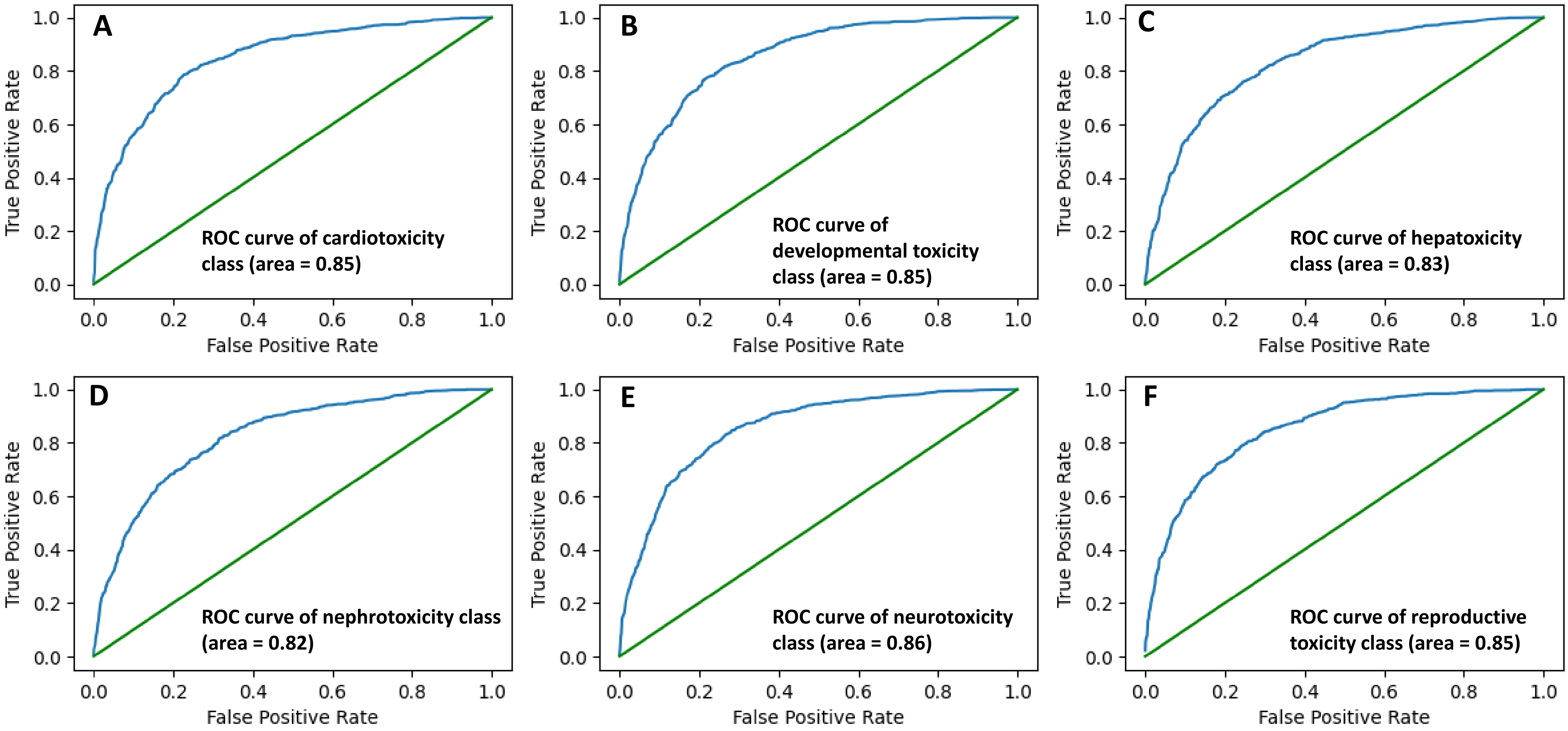

Chou, et al., unpublished results from the Lin Lab at UF.

Predictability of multi-task QSAR model for each toxicity endpoint

	ROC-AUC	BA	Precision	Recall	F1-Score
Cardiotoxicity	0.89	0.82	0.81	0.84	0.82
Developmental toxicity	0.90	0.84	0.83	0.82	0.83
Hepatoxicity	0.88	0.80	0.78	0.78	0.78
Nephrotoxicity	0.87	0.80	0.77	0.79	0.78
Neurotoxicity	0.88	0.82	0.86	0.87	0.87
Reproductive toxicity	0.89	0.82	0.74	0.80	0.76
Micro_Average	0.88	0.82	0.80	0.82	0.81

Note: Micro-averaging values computed a global average ROC-AUC, Balanced accuracy (BA), Precision Recall and F1 score by counting the sums of the True Positives (TP), False Negatives (FN), and False Positives (FP) for each of endpoints

Chou, et al., unpublished results from the Lin Lab at UF.

Summary of feature importance by using Extended-Connectivity Fingerprints (ECFPs) chemical descriptors and Tox21 assays

Tox21 assays related to organ toxicity:

- tox21-ache-p5_ache-inhibitor_1
- tox21-ap1-agonist-p1_ap1-agonist_1
- tox21-err-p1_err-antagonist_1
- tox21-herg-u2os-p1_herg-blocker_1
- tox21-ks-are-p1_nrf2-agonist_1
- tox21-p450-2c19-p1_2c19-inhibitor_1
- tox21-p450-2c9-p1_2c9-inhibitor_1
- tox21-p450-3a4-p1_3a4-inhibitor_1
- tox21-pgc-err-p1_pgc-err-antagonist_1
- tox21-pxr-p1_pxr-agonist_1
- tox21-shh-3t3-gli3-antagonist-p1_shh-antagonist_1

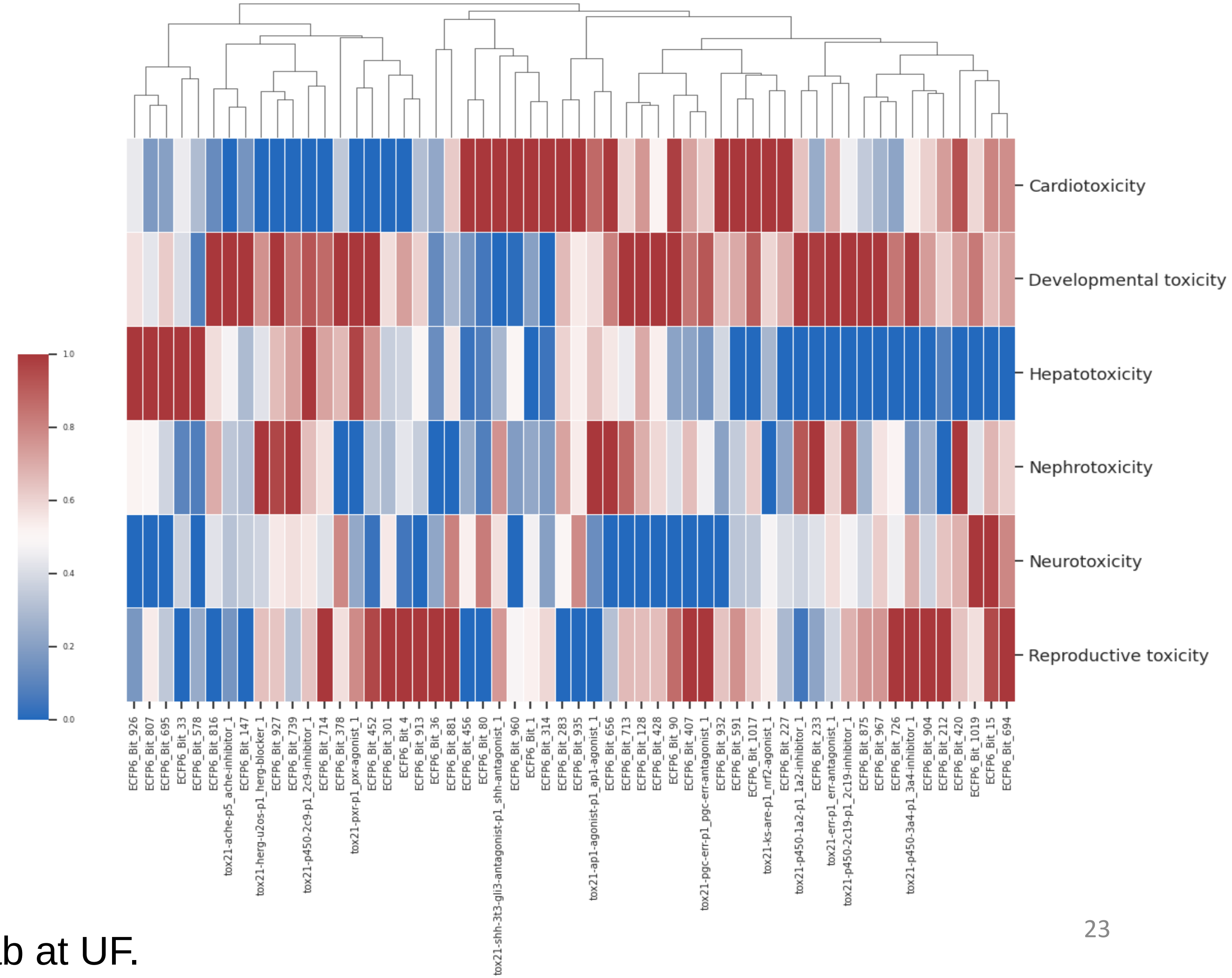

Chou, et al., unpublished results from the Lin Lab at UF.

Acknowledgements

Lab members:

Zhoumeng Lin
Wei-Chun Chou
Qiran Chen
Malek Hussein Hajjawi
Xue Wu
Kun Mi
Pei-Yu Wu
Chi-Yu Chen
Zhicheng Zhang
Venkata Nithin Kamineni
Yashas Kuchimanchi
Ethan Cecil

Former members:

Miao Li
Yi-Hsien Cheng
Md Mahbubul Huq Riad
Long Yuan
Dongping Zeng
Trevor Elwell-Cuddy
Paula Solar; Sichao Mao
Yilei Zheng; Yi-Jun Lin
Ning Xu; Yu Shin Wang
Jake Willson
Gabriel (Guanyu) Tao

Collaborators:

ICCM/NICKS/KSU
EGH/CEHT/UF
FARAD Team

Advisors:

Dr. Jim E. Riviere
Dr. Nancy A. Monteiro-Riviere
Dr. Nikolay M. Filipov
Dr. Jeffrey W. Fisher
Dr. Ronette Gehring

Funding:

- NIH/NIBIB Grant #: R01EB031022
- USDA/NIFA Award #: 2023-41480-41035
- USDA/NIFA Award #: 2022-41480-38137
- USDA/NIFA Award #: 2021-41480-35271
- USDA/NIFA Award #: 2021-67015-34084
- UF PHHP PhD Fellowship in Artificial Intelligence

National FARAD 2022

UF Lab 2023

UF Lab 2023